# REPORT DOCUMENTATION PAGE

Form Approved
OMB No. 0704-0188



| 1. REPORT DATE *(DD-MM-YYYY)* | 2. REPORT TYPE | 3. DATES COVERED *(From - To)* |
|---|---|---|
| | Technical Papers | |

**4. TITLE AND SUBTITLE**

**5a. CONTRACT NUMBER**

**5b. GRANT NUMBER**

**5c. PROGRAM ELEMENT NUMBER**

**6. AUTHOR(S)**

**5d. PROJECT NUMBER**
3058

**5e. TASK NUMBER**
RF9A

**5f. WORK UNIT NUMBER**

**7. PERFORMING ORGANIZATION NAME(S) AND ADDRESS(ES)**

Air Force Research Laboratory (AFMC)
AFRL/PRS
5 Pollux Drive
Edwards AFB CA 93524-7048

**8. PERFORMING ORGANIZATION REPORT**

**9. SPONSORING / MONITORING AGENCY NAME(S) AND ADDRESS(ES)**

Air Force Research Laboratory (AFMC)
AFRL/PRS
5 Pollux Drive
Edwards AFB CA 93524-7048

**10. SPONSOR/MONITOR'S ACRONYM(S)**

**11. SPONSOR/MONITOR'S NUMBER(S)**

**12. DISTRIBUTION / AVAILABILITY STATEMENT**

Approved for public release; distribution unlimited.

**13. SUPPLEMENTARY NOTES**

**14. ABSTRACT**

20030123 042

**15. SUBJECT TERMS**

| 16. SECURITY CLASSIFICATION OF: | | | 17. LIMITATION OF ABSTRACT | 18. NUMBER OF PAGES | 19a. NAME OF RESPONSIBLE PERSON |
|---|---|---|---|---|---|
| a. REPORT | b. ABSTRACT | c. THIS PAGE | | | Leilani Richardson |
| Unclassified | Unclassified | Unclassified | A | | 19b. TELEPHONE NUMBER *(include area code)* (661) 275-5015 |

Standard Form 298 (Rev. 8-98)
Prescribed by ANSI Std. 239.18

21 separate items enclosed

3058RF9A

0169A

✓DTIC

TP-FY99-0074

MEMORANDUM FOR PRS (Contractor/In-House Publication)

FROM: PROI (TI) (STINFO) 19 July 1999

SUBJECT: Authorization for Release of Technical Information, Control Number: AFRL-PR-ED-TP-FY99-~~0160~~ 0169A
Strakey, Talley, et al., "The Effects of LOX Post Biasing on SSME Injector Wall Compatibility"
**Journal submission** **(Statement A)**
AIAA Journal of Propulsion and Power

# THE EFFECTS OF LOX POST BIASING ON SSME INJECTOR WALL COMPATIBILITY

P. A. Strakey* and D. G. Talley†
Air Force Research Laboratory, 10 E. Saturn Blvd. Edwards AFB, CA 93524
&
L. K. Tseng‡ and K. I. Miner§
Boeing Rocketdyne Propulsion & Power, Canoga Park, CA

## Abstract

An experimental investigation has been carried out to examine the effects of LOX post biasing of a shear coaxial injector on the behavior of the spray near a chamber wall. The experimental work was performed with inert propellant simulants in a high-pressure chamber. Injector flow rates and chamber pressure were designed to match the Space Shuttle Main Engine (SSME) injector gas-to-liquid density and velocity ratio at the point of propellant injection. Measurements of liquid mass flux, gas phase velocity and droplet size were made using mechanical patternation and phase Doppler interferometry techniques. The measurements revealed that the liquid mass flux distribution shifts away from the wall with increasing LOX post bias away from the wall. The shift in the liquid flux distribution was much greater than that caused by the angling of the LOX post alone. Gas velocity near the wall simultaneously increased with increasing LOX post bias away from the wall. The increase in wall side gas velocity was due to the higher fraction of gas injected on the wall side of the injector as a result of the eccentricity at the injector exit. The net result was a decrease in mixture ratio near the wall. Estimates of heat transfer and engine performance relative to the unbiased case are presented.

## Introduction

The thrust of rocket propulsion technology today is to reduce engine costs while maintaining engine life and performance. One area of potential improvement in propulsion efficiency and engine lifetime is injector wall compatibility. In an effort to increase engine performance, chamber pressures have historically been increasing. The rate of heat transfer from the hot combustion gasses to the chamber wall is proportional to chamber pressure and in many cases results in a chamber wall temperature that is unacceptably high using regenerative cooling alone. This results in a need for additional wall cooling which is typically accomplished by increasing the fuel flow near the inside wall of the combustion chamber. The increased fuel flow reduces the mixture ratio near the wall, thereby decreasing the temperature of the combustion gasses. The increased fuel flow also provides a protective barrier against oxidizer attack on the chamber wall.

A number of methods have been developed and successfully implemented to provide gas or liquid film cooling protection for the combustion chamber wall. A commonly used method is the introduction of a row of holes in the injector faceplate very close to the chamber wall. These holes provide a curtain of protective film coolant, which can be either gaseous or liquid in phase. This technique can be applied to almost any type of injector configuration and has been used successfully for years in many LOX/kerosene impinging injector engines.

Another method of wall cooling which is particularly applicable to coaxial types of rocket injectors involves operating the outer row of injectors at a reduced mixture ratio either by increasing the fuel flow or by decreasing the oxidizer flow. The lower mixture ratio decreases the temperature of the combustion products near the wall. This is one type of wall protection that is employed in the SSME, which uses LOX/$gH_2$ shear coaxial injection elements. Another form of wall protection used in the SSME is the angling or "biasing" of the outer row of LOX posts inward, away from the combustion chamber wall. The biasing of the LOX post creates an eccentricity of the fuel annulus providing for a larger flowrate of gaseous fuel on the outer side of the injector. This arrangement, in conjunction with the decreased mixture ratio for the

---

* Research Scientist, Member AIAA
† Research Scientist, Member AIAA
‡ Engineer/Scientist, Combustion Analysis
§ SSME Development Engineer

outer row elements has been proven to provide adequate wall protection.

The price that is paid for protecting the wall by these methods is a loss in specific impulse ($I_s$) due to deviation in mixture ratio near the wall of the combustion chamber. It has been shown in a number of theoretical and experimental studies that any digression from the average mixture ratio in a combustion chamber results in a loss of performance, as measured by $I_s$.[1,2] This is true even when the overall engine mixture ratio is not at the optimum mixture ratio for maximizing $I_s$, as long as the $I_s$ versus mixture ratio curve is parabolic or similar in shape. This is the case with hydrogen and oxygen and most other propellant combinations. The sensitivity of performance to mixture ratio distribution in the combustion chamber is due to the relatively poor rate of mixing in the radial direction as a result of high axial acceleration rates of the combusting propellants, and short chamber lengths in comparison to the chamber diameter.

A study has been conducted at the Air Force Research Laboratory (AFRL) high-pressure cold-flow facility to increase the understanding of the injector wall interaction of a SSME shear coaxial injector. The goal was to provide a detailed understanding, through cold-flow simulations, of the effects of LOX post biasing on the liquid and gas phase distribution near a wall. Understanding the effects of LOX post biasing on the spray characteristics will allow injector designers to minimize the performance loss while still providing adequate wall protection.

## Experimental Setup

Water and gaseous nitrogen were used as simulants for LOX and gaseous hydrogen. In order to simulate the conditions inside the actual engine, the tests were performed at elevated pressure and at flow rates which match the hot-fire injection gas-to-liquid density and velocity ratios. Spray characteristics which were measured include liquid mass flux distribution, gas phase velocity and droplet size.

The experimental facility is capable of characterizing full scale single element rocket injectors in cold flow at pressures to 13.8 MPa. Water, which is used as a simulant for liquid oxygen, is stored and pressurized in a 1 $m^3$ tank. Nitrogen is stored in a 6 $m^3$ tank at 40 MPa. The injector gas and liquid flow rates are controlled with throttling valves and measured with turbine flow meters to an accuracy of +/- 1%. Chamber pressure is measured to within +/- 0.5%. The maximum water flow rate is 1.8 kg/s and the maximum nitrogen flowrate is 0.18 kg/s. The chamber consists of a 0.5 m diameter stainless steel, optically accessible pressure vessel containing a 27 tube linear array mechanical patternator which can be traversed through the spray. The patternator tubes are 6.35 mm square in dimension. A mechanical shutter prevents liquid from entering the tubes until the spray conditions are obtained at which time the shutter is opened and liquid is collected for a specified amount of time in a series of stainless steel bottles connected to the patternator tubes. After the shutter has closed, the bottles are de-pressurized and the liquid is emptied into beakers and weighed. The mass flux is simply the mass of collected fluid divided by the collection time and cross sectional are of the collection tubes. The patternator was traversed through the spray at 6.35 mm steps, thus yielding a two-dimensional map of the liquid mass flux distribution.

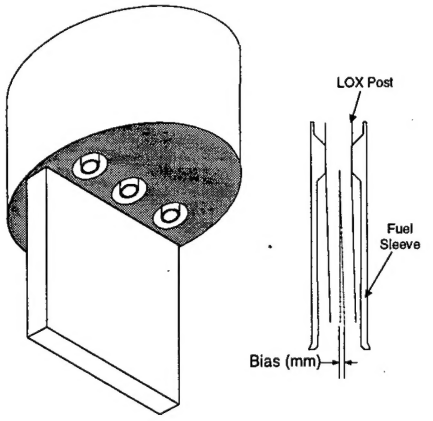


**Figure 1: Schematic of the 3-element SSME injector and wall test article along with a cutaway of an injector element.**

Three 50 mm and one 120 mm sapphire windows provided optical access to the chamber for spray imaging and for droplet size and velocity measurements using phase Doppler interferometry (PDI).

The injector, which was designed and manufactured by Boeing Rocketdyne, consisted of a stainless steel manifold containing three SSME fuel sleeves and LOX posts. The manifold provided separate inlet ports for gas and liquid delivery. A wall was mounted on the face of the manifold at 6.35 mm from the outside edge of the fuel sleeves to simulate the presence of the combustion chamber wall. The LOX posts had an internal diameter of 4.77 mm and the fuel gap annulus was 2.24 mm with the LOX post centered in the annulus. Figure 1 is a schematic of the injector manifold along with a cross sectional view of one of the

injector elements. The LOX posts were biased by angling the posts away from the wall. Bias was measured as the displacement of the tip of the LOX post from the unbiased condition.

## Injector Scaling Parameters

Chamber pressure and flow rates were chosen to match the following SSME injector hot fire similarity parameters at the point of injection: gas-to-liquid velocity ratio, density ratio, momentum ratio and mixture ratio, while the maximum gas flowrate was limited by the maximum facility flowrate. Table 1 contains the single element run conditions used in this study along with conditions for the SSME at full power level. The most notable difference between cold-flow and the SSME hot-fire conditions was the lower liquid Reynolds number for the cold-flow tests, which was lower by a factor of 25 due to the lower injection velocity and a seven-fold higher viscosity for water. The results should still provide qualitative information on spray behavior because the Reynolds number for the cold-flow tests was still well into the fully turbulent regime. For all of the results presented here, all three injectors were flowing $gN_2$ at the flow rate specified in Table 1, however, water was flowed through only the central injector. This was an effort to reduce the optical thickness of the spray field in order to facilitate the droplet size and velocity measurements. The gas flow in the outer two injectors was designed to simulate the aerodynamic confinement encountered in the actual engine.

**Table 1 : Scaling parameters for cold-flow and engine operating conditions.**

| Parameter | SSME (LOX/ $gH_2+H_2O$) | Cold-Flow ($H_2O$/ $N_2$) |
|---|---|---|
| Chamber Pressure (MPa) | 19.3 | 0.74 |
| Liq. Flowrate (kg/s) | 0.63 | 0.18 |
| Liq. Injection Vel. (m/s) | 31.3 | 10.0 |
| Liq. Density ($kg/m^3$) | 1117 | 1002 |
| Liq. Reynolds Number | $1.1 \times 10^6$ | $4.3 \times 10^4$ |
| Gas Flowrate (kg/s) | 0.193 | 0.056 |
| Gas Injection Vel. (m/s) | 360.6 | 115.9 |
| Gas Density ($kg/m^3$) | 9.47 | 8.48 |
| Gas Reynolds Number | $9.0 \times 10^5$ | $2.4 \times 10^5$ |
| Density Ratio (liq/gas) | 117.6 | 117.6 |
| Velocity Ratio (liq/gas) | 0.087 | 0.087 |
| Momentum Ratio (liq/gas) | 0.286 | 0.286 |
| Mixture Ratio (liq/gas) | 3.25 | 3.25 |

## Results and Discussion

### Strobelight Imaging

Spray imaging experiments were conducted at a variety of test conditions using a 5 μs duration strobelight to back-light the spray and a CCD camera and VCR to capture and store images of the spray. These images yielded qualitative information on the shape of the sprays. A series of images were taken at the conditions listed in Table 1 for an unbiased injector and for a biasing of 0.48 mm away from the wall. The images in Figure 2 show the spray from the edge on and span an axial distance of 0 to 45 mm (top row) and 45 to 110 mm (bottom row). Note that each image in the top and bottom row series of images was captured at a different instance in time and are therefore representative of typical spray behavior. The dark areas on the image are areas with a high liquid concentration. These images indicate that biasing the LOX posts tended to shift the liquid flow away from the wall.

### Liquid Mass Flux Results

Mechanical patternation measurements of liquid mass flux were made with all three injectors flowing $N_2$ and only the central injector flowing water. Tests were conducted with the LOX posts unbiased (centered in the fuel sleeve) and with the LOX post tips biased away from the wall 0.25, 0.48 and 1.02 mm. Figure 3 contains contour plots of measured liquid mass flux at axial locations of 51, 83 and 127 mm from the injector exit plane. The wall was located at 0.0 mm and the center of the injector was located at 10 mm from the wall. These results show a decrease in liquid flux near the wall and a shift in the peak mass flux away from the wall as the LOX posts were biased away from the wall. The shift in the peak flux was largely due to an increase in gas flow on the wall side of the biased injectors, which will be discussed in a later section.

Figure 4 is a plot of liquid mass flux as a function of distance from the wall through the centerline of the spray. The size and location of the injector is shown in the figure. Figure 4 clearly shows the shift in the peak of the liquid flux distribution away from the wall with increasing LOX post bias. It is interesting to note that the maximum liquid flux displacement occurs for a biasing of 0.48 mm. Further biasing to 1.02 mm did not shift the liquid flux any further away from the wall. Also note that the effect of LOX post biasing diminished with increasing axial distance from the injector.

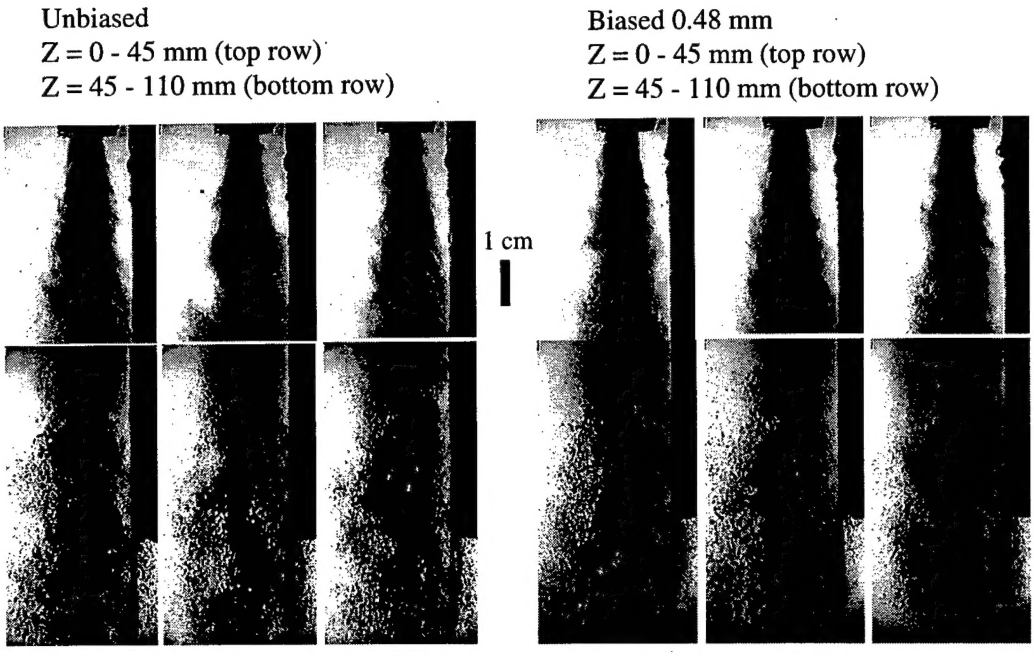


**Figure 2: Strobe back-lit images of the unbiased injector spray (left) and biased injector spray (right) at two axial locations. The wall is the dark object located on the right hand side of each image.**

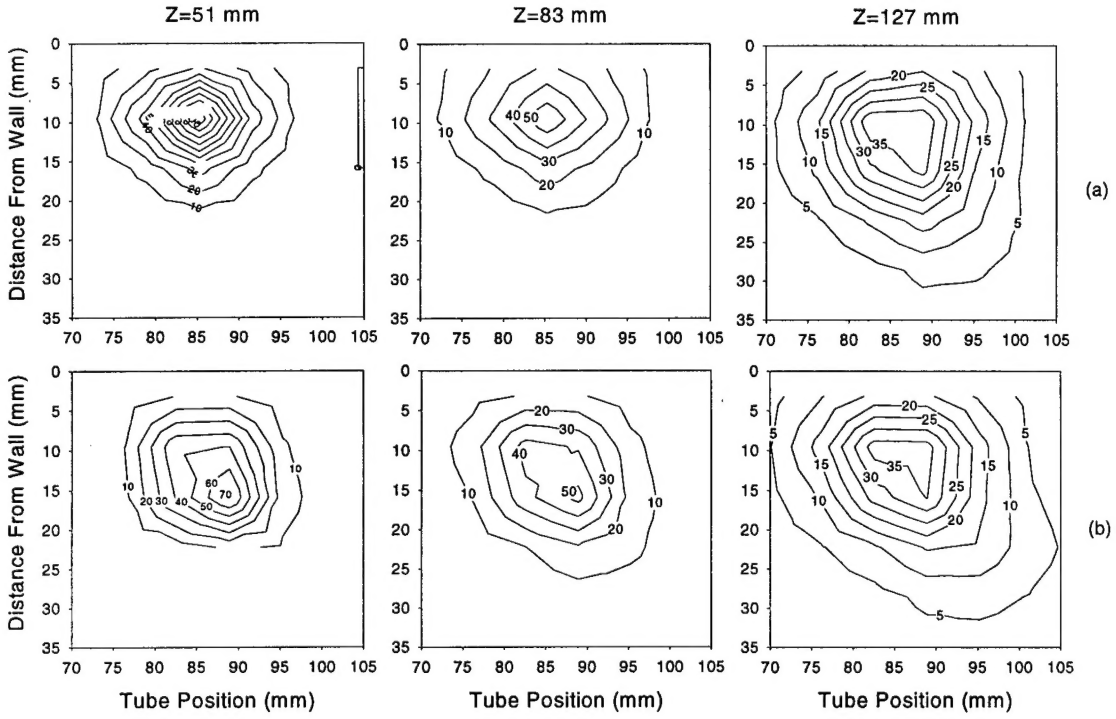


**Figure 3: 2-D liquid mass flux distributions at Z=51, 83 and 127 mm, for the test conditions in Table 1 for the (a) unbiased injector and (b) injector biased 0.48 mm away from the wall. The wall is at 0 mm and contours are in gm/s/cm$^2$.**

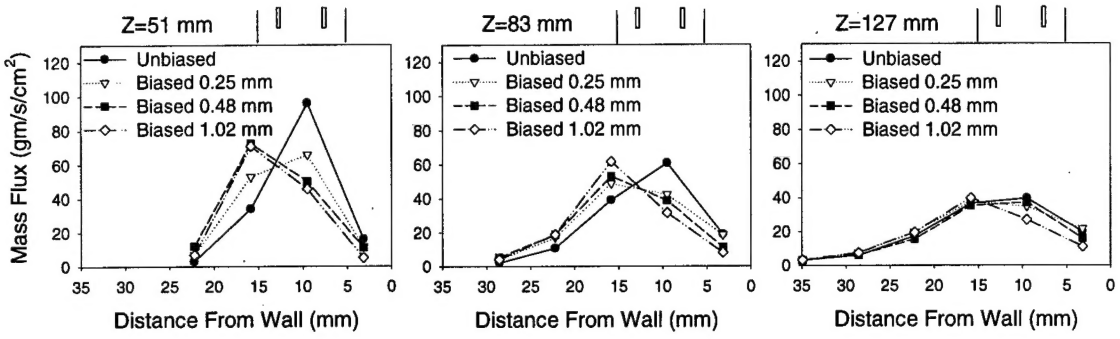


**Figure 4: Liquid mass flux distribution through the centerline of the spray as a function of LOX post biasing and axial distance. Run conditions listed in Table 1.**

The shift in the peak of the liquid mass flux distribution was much greater than that caused by only the angling of the LOX post. For the case of 0.48 mm bias, the LOX post biasing angle was 0.69°, which would result in a shift of 0.61 mm away from the wall at an axial location of 51 mm. The actual shift in the peak as determined by curve fitting the liquid flux data to a Gaussian profile was 3.9 mm.

## Estimation of Error

Several repeat runs were made with the injector biased at 0.48 mm in order to assess the repeatability of the liquid mass flux measurements. The error associated with repeatability varied slightly through the spray but the average standard deviation in liquid mass flux was about 7%. Another error associated with mechanical patternation measurements is rejection of droplets at the entrance of the patternaor tubes due to the formation of a stagnation zone. The patternator bottles were vented back to chamber to allow the gas that enters the collection tubes to return to the chamber. There was, however a pressure drop through the patternation system that generates a stagnation zone at the entrance to the patternator tubes. The smaller droplets tend to follow the gas streamlines around the patternator entrance and are not collected. Larger droplets, which carry most of the mass flux in the spray have enough momentum in the axial direction to overcome the streamlines formed by the stagnation zone and enter the patternator. The amount of error associated with droplet rejection can be assessed by integrating the total mass flux over the extent of the spray and comparing to the injected mass flow rate. The result is a collection efficiency, which will always be less than 100%. The measured collection efficiency for the unbiased and biased runs were similar, but varied in the axial direction. The average collection efficiency was 71%, 80% and 87% for the axial locations of 51, 83 and 127 mm respectively. Collection efficiency increased with increasing axial distance from the injector as the local gas velocity decreased.

## Velocity Measurements

Gas phase velocity and liquid droplet size measurements were made with a 2-component phase Doppler interferometer (PDI). Measurements were made with the PDI at axial locations of 51, 83 and 127 mm. The PDI was optically configured to measure the smallest droplets possible. It was calculated that droplets less than about 6 μm in diameter would be following the mean flowfield completely and could be used as "seed" particles for making measurements of the gas phase velocity. The requirement was that the droplet relaxation time, $\tau_D$, be much less than the characteristic mean timescale for the flowfield, $\tau_F$. The relationship used here was;

$$\frac{\tau_D}{\tau_F} < 0.1 \tag{1}$$

The droplet relaxation time is the time lag for a droplet to accelerate from the injected liquid velocity to the mean flowfield velocity. $\tau_F$ and $\tau_D$ are calculated as follows.

$$\tau_F = \frac{Z}{V} \tag{2}$$

$$\tau_D = \frac{\rho_l \cdot D^2}{18 \cdot \mu_g} \tag{3}$$

In Equation 2, Z is the minimum distance from the injector and V is the maximum flowfield velocity. At a distance of 51 mm the maximum flowfield velocity was estimated to be 50 m/s from initial

experiments. This yielded a time constant, $\tau_f$, of 1.02 ms and a droplet size, D, of 5.7 μm for $\tau_D/\tau_F=0.1$

Measurements were also made as close as 5 mm from the injector face, but there were very few droplets available for making velocity measurements here, therefore the gas stream being fed to the injector was seeded with a dilute spray of very small droplets to act as tracer particles. The introduction of droplets to the gas flow was far enough upstream of the injection point to ensure that the droplets were following the flowfield.

The PDI was configured with a 500 mm focal length transmitter and receiver lens. A 60 μm beam waist and a 50 μm slit were used in order to facilitate measurements in the anticipated high number density sprays. A ten-to-one intensity validation scheme was implemented to reject erroneous measurements associated with the relatively small beam waist in comparison to the droplet sizes being measured ($2<D<350$ μm).[3]

The PDI was fixed in location with respect to the chamber windows and the injector was traversed through the probe volume at 1 mm steps for the axial location of 5 mm and 3 mm steps for all other axial locations. This yielded a radial profile of the gas phase velocity and droplet diameter from the outside edge of the spray to the wall, through the centerline of the spray as defined by the center of the LOX post. At each location in the spray, 5000 measurements were recorded. Velocities are reported as the average velocity of droplets less than 6 μm in diameter. It was found, however, that there was very little correlation between droplet size and velocity, indicating that velocity was independent of droplet size.

Figure 5 contains plots of gas phase axial velocity as a function of distance from the wall at axial locations of 5, 51, 83 and 127 mm for the test conditions listed in Table 1. The relative size and location of the injector is shown on each plot. Figure 5 shows that near the exit of the injector (Z=5 mm) the gas phase velocity was only slightly higher on the wall

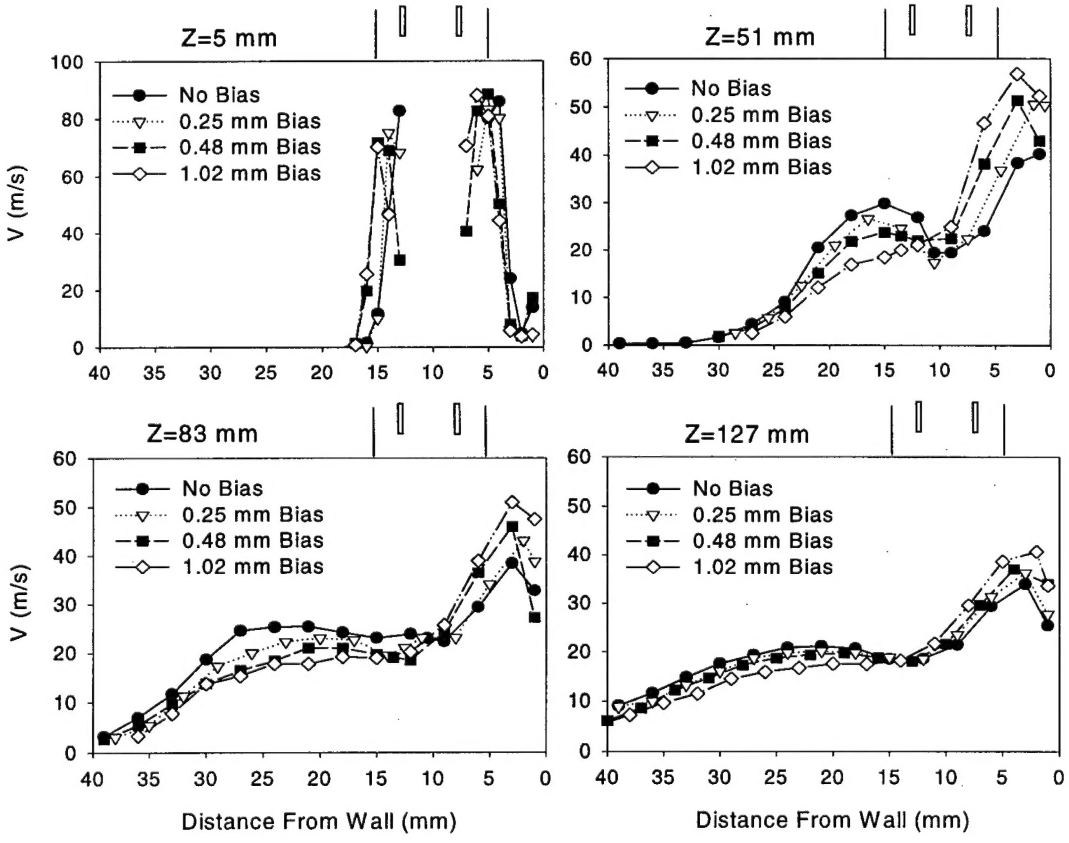


**Figure 5: Gas phase axial velocity profiles versus distance from the wall at axial locations of 5, 51, 83 and 127 mm. Profiles are through the centerline of spray as defined by the LOX post and the injector is shown schematically in the plots.**

side of the injector than the far side of the injector. Note that at the axial location of Z=5 mm, no data is shown in the center of the spray. This is due to the fact that at this axial location the liquid core of the spray was still intact and data validation rates at these locations were very low. Further downstream from the injection point the gas phase axial velocities were much higher on the wall side of the spray than the far side of the spray. This is because the spray was physically confined by the presence of the wall at 0 mm and was aerodynamically confined by the injectors operating on either side of the spray. The far side of the spray was not confined and was free to expand, thus resulting in a lower velocity.

The most interesting feature of Figure 5 is the increase in velocity near the wall with a corresponding decrease in velocity on the far side of the spray for the runs with the LOX post biased away from the wall. The ratio of wall side velocity to far side velocity increased with increasing LOX post bias. The velocity gradient was caused by the unequal exit areas of the gas annulus at the injector exit, with a larger flow area on the wall side of the injector. Since the flow was physically confined on the wall side of the injector, the wall side velocity must increase as the injector exit area and hence flow rate increased with bias. The effect of biasing was most prominent at the 51 mm axial location, with a decrease in relative effect as the spray evolved in time (axial distance) from the point of injection. The decrease in influence of the LOX post bias on the velocity distribution with increasing axial distance was a result of transport and mixing of the unevenly distributed gas on the wall side of the spray to the far side of the spray due to the large axial velocity gradient in the radial direction. This was the driving force behind the shift in the liquid phase away from the wall in Figure 4.

In order to calculate the liquid-to-gas mixture ratio from the liquid flux and gas phase velocity data, which were collected at different spatial resolutions, the liquid flux data were curve fit to a Gaussian profile and the mixture ratio was calculated at the data points corresponding to the gas phase velocity measurements. The mixture ratio distribution for the unbiased and biased injectors is shown in Figure 6. The shift in mixture ratio away from the wall was most prominent at the axial location of 51 mm, but persisted even at the 127 mm location. The shift in mixture ratio was due to the combined effect of the shifting of the liquid flux distribution away from the wall, and the increased gas flow near the wall. The total measured mixture ratio for each run was significantly less than the injected mixture ratio of 3.25 due to entrainment of chamber gas into the spray. The amount of entrained gas increased with increasing distance from the point of injection.

## Heat Flux Analysis

One of the goals of the present investigation is to use the experimental cold-flow data to estimate the effects of LOX post biasing on wall heat transfer and engine performance in the SSME. Since the engine operates fuel rich, any reduction in mixture ratio near the wall might imply a decrease in hot gas temperature and heat transfer to the wall. Two approaches were used to predict relative changes in heat transfer between the unbiased and biased injector data. The first approach incorporated a flat plate turbulent heat transfer correlation (Equation 4) using the measured gas velocity and mixture ratio near the wall.[4]

$$q'' = 0.0296 \mathrm{Re}_z^{\frac{4}{5}} \mathrm{Pr}^{\frac{1}{3}} \frac{k_g}{Z}(T_g - T_w)$$
$$\mathrm{Re}_z = \frac{V_g \rho_g Z}{\mu_g} \qquad (4)$$

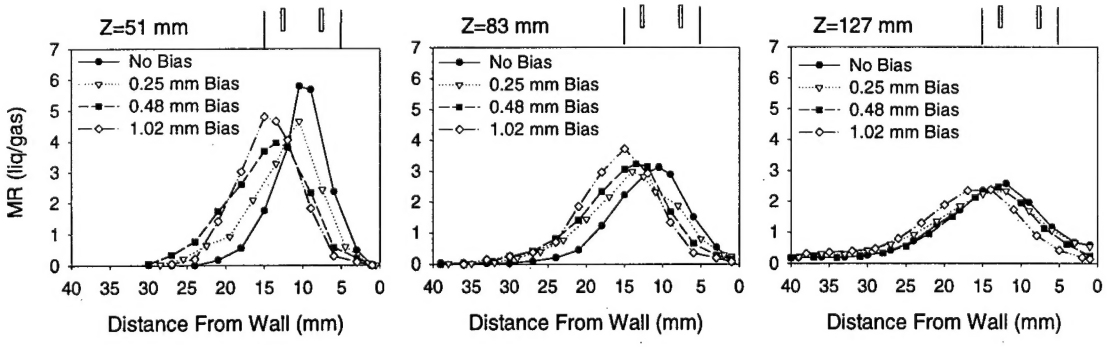


**Figure 6: Mixture ratio distribution for unbiased and biased injectors at axial locations of 51, 83 and 127 mm. Injector size and location is shown on the plots. Test conditions are given in Table 1.**

**Table 2: Relative change in heat transfer for biased data.**

| Biasing (mm) | Δq" @Z=51 mm | Δq" @Z=83 mm | Δq" @Z=127 mm |
|---|---|---|---|
| 0.25 | -8% | -4% | -4% |
| 0.48 | -7% | -20% | -14% |
| 1.02 | -11% | -28% | -29% |

Local gas temperature and transport properties were calculated using the NASA CEA chemical equilibrium code using the mixture ratio data from Figure 6. A constant wall temperature of 600 K was assumed in the calculation for both the unbiased and biased data. The heat flux was averaged from 1 to 6 mm from the wall, which was estimated to be the extent of the thermal boundary layer at the throat of the SSME using Equation 5.

$$\delta_t = 0.37 \cdot Z \cdot \mathrm{Re}_z^{\frac{-1}{5}} \qquad (5)$$

The average Reynolds number in the SSME combustion chamber is estimated to be about $5 \times 10^6$ which yielded a boundary layer thickness of 6 mm at the throat. The calculated heat fluxes for the biased runs were expressed as a percent change from the unbiased data and are tabulated in Table 2.

It is interesting to note that the maximum reduction in heat transfer occurred further downstream with increasing LOX post bias. In the SSME the outer row of injectors contain LOX posts which are biased 0.48 mm inward. The predicted decrease in heat transfer from the cold-flow data is 7% at the 51 mm axial location, increasing to 20% then dropping off to 14% at the 127 mm axial location.

The second method of predicting heat transfer from the cold-flow data involved a manipulation of sub-scale hot-fire test data obtained with a calorimeter test chamber and unbiased injectors. The calorimeter test data provided a profile of heat flux as a function of axial location between the injector faceplate and the chamber throat. Heat flux data obtained with unbiased injectors was adjusted by the relative change in gas velocity and mixture ratio near the wall between the biased and unbiased cold-flow data. The effect of mixture ratio and velocity on heat transfer was assumed to be similar to the previous method using a flat plate heat transfer correlation. The effect of biasing (for the 0.48 mm biased data), as measured with the cold-flow experiments was then extrapolated to the chamber throat to obtain an integrated heat load reduction of 7.1%, which agrees very well with full-scale engine test data. The main difference between these two methods of predicting heat transfer is that method 1 provides a measure of relative heat flux at several axial locations, while method 2 provides a prediction of overall heat load change.

## Performance Analysis

The most commonly used method of estimating the performance impact of mixture ratio non-uniformity in a rocket engine is stream-tube analysis. The assumption is that there is negligible mixing between adjacent injectors and therefore the performance of each injector can be calculated separately and summed to obtain the total engine performance, which can be measured by specific impulse. The use of stream-tube analysis to predict engine performance has been validated with a large database of experimental hot-fire data.[5] A schematic representation of stream-tube analysis is given in Figure 7 which shows that each injector element is assumed to operate over an equal area of the combustion chamber and does not mix with adjacent elements.

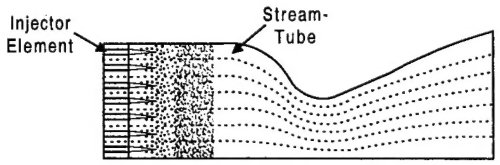


**Figure 7: Schematic representation of stream-tube analysis.**

The SSME injector consists of 600 elements, 515 of which are unbiased "core" elements and 85 of which are biased "wall" elements. Each of the core elements constituted 1 stream-tube, while each of the wall elements was subdivided into two sub-stream-tubes representing the wall side of the spray and the far side of the spray. The dividing line that defines the center of the spray was taken to be at the point of maximum liquid flux as measured with the cold-flow experiments. Since the shape of the liquid flux distributions for all of the runs was very similar, the relative amount of gas flow on each side of the spray was assumed to be the only factor in skewing the mixture ratio from the unbiased condition. $I_s$ was calculated by assuming that the unbiased data represented a case of perfect mixing at the injected mixture ratio, and the biased data represented a deviation from perfection by the amount of gas flow on

each side of the spray relative to the unbiased condition. Vacuum $I_s$ was calculated using the NASA CEA chemical equilibrium code for the injected propellants. The oxidizer was LOX at 122 K, while the fuel is a mixture of 55% gaseous hydrogen and 45% water vapor by weight at approximately 800K. Note that the mixture ratio was defined as the ratio of oxidizer to fuel, not oxygen to hydrogen. The calculated vacuum $I_s$ as a function of mixture ratio and LOX to $H_2$ ratio is provided in Figure 8. In the SSME the outer row of injectors operate at a LOX to hot gas mixture ratio of 3.0 while the core injectors operate at 3.4. The overall LOX to $H_2$ ratio for the SSME is about 6.0.

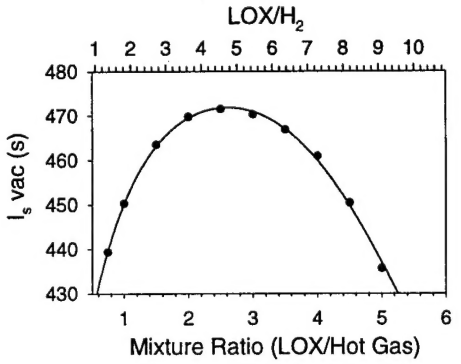


**Figure 8 : Vacuum $I_s$ versus mixture ratio and LOX-to $H_2$ ratio for the SSME.**

The calculated vacuum $I_s$ for each side of the spray was multiplied by the mass fraction ($m_f$) of propellant on each side of the spray and summed to obtain the total $I_s$ within the stream-tube. The total $I_s$ for the engine was calculated in a similar fashion, by summing the $I_s \cdot m_f$ of all 600 individual stream-tubes.

The calculated $I_s$, expressed as a change from the unbiased condition is given in Table 3 as a function of LOX post biasing at each axial location. Each axial location represents a calculation of performance assuming that location represents the overall state of mixing in the engine. Many researchers have made direct comparisons between cold-flow and hot-fire data at equivalent axial locations. A study with gaseous oxygen and gaseous hydrogen propellants has suggested that the fraction of heat released in an engine is roughly equal to the cold-flow mixing efficiency at equivalent residence times from the point of injection.[6] For the SSME, the total chamber residence time is approximately 1 ms, which would most closely match the cold-flow data at the 51 mm location. The $I_s$ calculations at other axial locations are provided as an estimation of the range of $I_s$ losses that could be expected with LOX post biasing.

Also provided in the last column of Table 3 is an estimate of $I_s$ loss from a method similar to the one just described, but where the amount of gas flow on each side of the spray was assumed to be equal to the relative cross-sectional area of the gas annulus at the LOX post tip. The flow was divided at the center of the LOX post. This analysis did not use any of the cold flow data. It is interesting that this simple analysis agrees well with the analysis based on cold-flow data (highlighted in bold) at an axial location that decreases with increasing LOX post bias. All of the performance loss estimates for the case of 0.48 mm (SSME) show that the amount of $I_s$ loss is very small and is probably too small to verify with full scale engine test data.

In an effort to find the optimum LOX post bias for minimizing heat transfer while maximizing $I_s$ , the heat transfer data from Table 2 was normalized by the percent decrease in $I_s$ from Table 3, and is shown in Figure 9 for the three different axial locations. The peak of each curve in Fig. 9 represents the LOX post bias at which the heat transfer to $I_s$ loss ratio is optimized. Although the 83 and 127 mm data were optimized at a bias of 0.48 mm, the 51 mm data was optimized at a bias of 0.25 mm. It is possible that the overall injector optimum operating point is somewhere between the two.

## Droplet Size Measurements

Droplet size measurements were made with the PDI technique described previously. Droplet size data is presented for the axial location of 127 mm in Figure 10 in the form of the volume mean diameter, $D_{30}$. Droplet size data is shown only for the locations where the data validation rates where relatively high (> 60%) and the PDI measured mass flux agreed

**Table 3: $I_s$ change from unbiased condition from cold-flow data analysis and from injector area analysis (last column).**

| Biasing (mm) | $\Delta I_s$ (s) @Z=51 mm | $\Delta I_s$ (s) @Z=83 mm | $\Delta I_s$ (s) @Z=127 mm | $\Delta I_s$ (s) |
|---|---|---|---|---|
| 0.25 | -0.2 | -0.25 | **-0.13** | -0.14 |
| 0.48 | -0.63 | **-0.50** | -0.27 | -0.45 |
| 1.02 | **-2.18** | -1.08 | -0.87 | -2.10 |

relatively well with the patternator data. In the core of the spray at Z=127 mm, as well as with the shorter axial locations, the presence of large, non-spherical ligaments was believed to be the cause of low data validation rates. The presence of large ligaments is supported by the images in Figure 2.

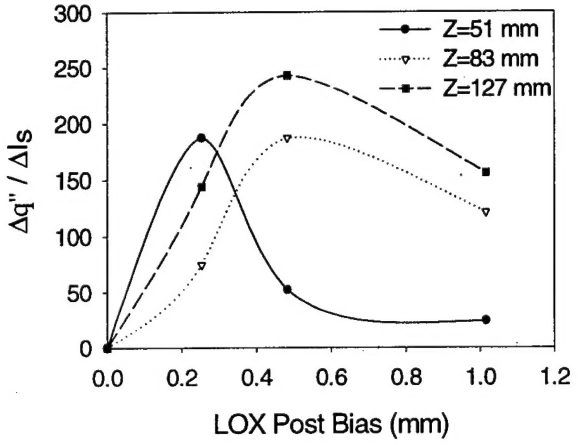


**Figure 9: Percent change in heat flux normalized by the percent change in $I_s$ as a function of LOX post bias at Z=51, 83 and 127 mm.**

Figure 10 shows an increase in $D_{30}$ on the side of the spray away from the wall with increasing LOX post bias. This was believed to be due to the decrease in gas velocity, and hence, Weber number on this side of the spray as shown in Figure 5. There was also a corresponding decrease in droplet size on the wall side of the spray with increasing LOX post bias.

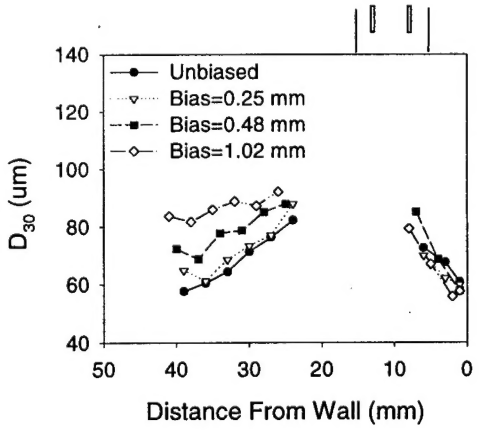


**Figure 10: Volume mean diameter versus distance from wall as a function of LOX post bias at Z=127 mm. Test conditions from Table 1. Size and location of injector shown on plot.**

## Conclusions

The cold-flow measurements have shown a pronounced effect of LOX post biasing on the mixture ratio distribution near the wall. This was largely the result of the increased gas flow on the wall side of the injector. It is this decrease in mixture ratio, and hence combustion temperature, along with a decrease in LOX flow near the wall that provides the protection to the wall of the SSME combustion chamber.

The optimization curves in Figure 9 provide the injector designer with information on how to design a biased injector but do not guarantee that an optimized injector will provide adequate wall protection. Maximum tolerable wall temperature might dictate that the injector be designed far from optimum. The implication for the SSME is that some reduction in the amount of biasing in the outer of injectors might recover some performance loss while still maintaining an acceptable wall temperature.

Droplet size measurements showed a decrease in droplet size near the wall with increasing LOX post bias and a corresponding increase in droplet size on the far side of the spray. The effect on droplet size is probably too small to have a measurable impact on engine performance or heat transfer.

These results will allow injector designers to better predict heat transfer and performance impact in new engines and reduce the amount of time spent in the hot-fire testing and redesign phase of an engine development program.

## Nomenclature

| | |
|---|---|
| D | droplet size (m) |
| h | heat transfer coefficient ($W/m^2/K$) |
| $I_s$ | specific impulse (s) |
| $k_g$ | thermal conductivity (W/m/K) |
| $m_f$ | mass fraction |
| MR | mixture ratio (liq/gas) |
| Pr | Prandtl number |
| q" | heat flux ($W/m^2$) |
| $T_g$ | gas temperature (K) |
| $T_w$ | wall temperature (K) |
| $V_g$ | gas velocity (m/s) |
| Z | axial distance (from injector) (m) |
| $\rho_l$ | liquid density ($kg/m^3$) |
| $\rho_g$ | gas density ($kg/m^3$) |
| $\mu_g$ | gas viscosity ($N\ s/m^2$) |

## Acknowledgments

The authors would like to thank Mr. Mike Griggs and Mr. Timothy Auyeung for their assistance in operating the facility and collecting data.

## References

1. K. Ramamurthi and A. Jayashree, "Optimization of Mixture Ratio Distribution in Liquid Propellant Rocket Thrust Chamber", *Journal of Propulsion and Power*, Vol. 8, No. 3, May-June, 1992, pp. 605-608.

2. J. L. Pieper, L. E. Dean and R. S. Valentine, "Mixture Ratio Distribution- Its Impact on Rocket Thrust Chamber Performance", *Journal of Spacecraft and Rockets*, Vol. 4, No. 6, June 1967, pp. 786-789.

3. P.A. Strakey, D.G. Talley, W.D. Bachalo and S.V. Sankar, "The Use of Small Probe Volumes with Phase Doppler Interferometry" Presented at the 12th International Conference of ILASS-Americas, Sacramento, CA, May 17-20, 1998.

4. Fundamentals of Heat and Mass Transfer, Incropera and DeWitt, Wiley and Sons, New York, 1985, pg. 319.

5. Nurick, W. H. And Clapp, S. D., "An experimental Technique for Measurement of Injector Spray Mixing", *Journal of Spacecraft and Rockets*, Vol. 6, No. 11, Nov. 1969, pp. 1312-1315.

6. D. F. Calhoon, D. L. Kors and L. H. Gordon, "An Injector Design Model for Predicting Rocket Engine Performance and Heat Transfer" AIAA Paper No. 73-1242, AIAA/SAE 9th Propulsion Conference, Las Vegas, Nevada, Nov. 5-7, 1973.